Chapter

5

In preparation

Silencing of Pericyte MicroRNA-132 Reduces Renal Fibrosis and Myofibroblast Proliferation and is Associated with Altered Sirt1 and Cox2 Expression

R. Bijkerk[1,2], C. van Solingen[1], R.G. de Bruin[1], J.M.G.J. Duijs[1], T.J. Rabelink[1], B.D. Humphreys[2] and A.J. van Zonneveld[1]

[1]Department of Nephrology and the Einthoven Laboratory for Experimental Vascular Medicine, Leiden University Medical Center (LUMC), Leiden. [2]Renal Divison, Department of Medicine, Brigham & Women's Hospital and Harvard Medical School, Boston, Massachusetts, USA.

Abstract

Lineage analysis has shown that during nephrogenesis, FoxD1-positive mesenchymal cells give rise to adult interstitial pericytes. These FoxD1-derivative interstitial cells expand and differentiate into smooth muscle actin (α-SMA) positive myofibroblasts during renal fibrosis, accounting for a large majority of myofibroblasts. MicroRNAs (miRNAs) involved in this differentiation could serve as a target to decrease myofibroblast formation in fibrotic kidney disease. To identify miRNAs differentially expressed in myofibroblasts we induced fibrosis in FoxD1-GC;Z/Red mice by unilateral ureteric obstruction (UUO). Subsequently, dsRed positive cells were isolated using FACS sorting and used for miRNA profiling. MiR-132 was amongst the most highly upregulated miRNAs in the dsRed positive cells in the fibrotic kidney. In vitro we demonstrated that silencing miR-132 results in reduction of myofibroblast marker α-SMA, reduced proliferation and increased levels of its established target Sirt1 and downstream Cox2. In vivo silencing of miR-132 by antagomirs directed to miR-132 in the UUO model resulted in a 35% decrease in collagen deposition and decreased tubular apoptosis after 10 days as compared to scramblemir controls, while no difference was observed yet after 5 days. IHC analysis demonstrated that the number of interstitial α-SMA positive cells was similarly decreased, which could be confirmed by both western blot and qRT-PCR analyses. No difference was observed in capillary density. Furthermore, we demonstrated that miR-132 silencing is associated with decreased Sirt1 and Cox2 expression and decreases the number of proliferating interstitial cells. Silencing miR-132 protects counteracts the progression of renal fibrosis, decreases myofibroblast proliferation and is associated with strongly altered Sirt1 and Cox2 levels.

Introduction

Pericytes are stromal cells that are known to cover and support capillary walls. Lineage tracing of pericyte cell fate using FoxD1-Cre;Rosa26R mice demonstrated that these perivascular cells are the major source of α-SMA positive myofibroblasts in mouse models of renal fibrosis[1,2].

MicroRNAs (miRNAs) are small ~22 nt RNAs and constitute a class of highly conserved non-coding RNAs hat control gene expression by inhibiting the translation of mRNA[3]. MiRNAs are able to regulate multiple targets and thereby provide a means for the coordinated control of gene expression. As a consequence, these molecules are attractive candidates for regulating cell type-specific differentiation and modulating cell function[4].

Several reports already established a role for miRNAs is the development of tissue fibrosis. In the failing heart miR-21 levels are increased in fibroblasts and *in vivo* silencing of miR-21 by antagomirs reduces cardiac ERK-MAP kinase activity and interstitial fibrosis[5]. Likewise, miR-133[6] and cardiac specific miR-208[7] have been involved in the pathogenesis of fibrosis in the heart. In addition, members of the miR-29 family have been described in fibrosis. In a myocardial infarction model it was shown that members of the miR-29 family are down regulated and miR-29 silencing with anti-miRs *in vitro* and *in vivo* induced the expression of collagens, whereas over expression of miR-29 in fibroblasts reduced collagen expression[8]. Also in the liver members of the miR-29 family were shown to be downregulated in fibrosis[9]. In kidneys from rats, knockdown of miR-29b resulted in upregulation of several collagen genes[10].

In the kidney, several miRNAs (miR-21, -214, -324-3p, 382) are now recognized to be important mediators in the development of renal fibrosis[11-15]. Also miR-192 is involved as a tight association was demonstrated of miR-192 expression in the kidney with both activation of TGF-beta/Smad signaling[16,17], as well as with tubulo-interstitial fibrosis and low estimated glomerular filtration rate (GFR) in diabetic nephropathy patients[18].

As pericytes are considered to be the main source of myofibroblasts, we aimed to identify miRNAs that play an important role in the process of myofibroblast formation from pericytes in renal fibrosis. To this end, we used a FoxD1-GC;DsRed mouse model to genetically label pericytes and subsequently isolated these cells through FACS-sorting from healthy kidneys

and fibrotic kidneys that were exposed to unilateral urether obstruction (UUO). Following miRNA profiling of the isolated cells we found miR-132 to be dramatically increased. Since miR-132 has been described to directly target NAD-dependent deacetylase Sirt1[19] and Sirt1 is known to protect against renal fibrosis[20] we further investigated the role of this miRNA in renal fibrosis and related its expression to SIRT1 activity. We demonstrated that silencing of miR-132 reduces the fibrotic response in a UUO model of renal fibrosis predominantly by decreasing the proliferative capacity of pericyte-derived myofibroblasts.

Results

Accumulation of FoxD1-derivative interstitial cells in UUO in mice

To follow the fate of pericytes in the pathogenesis of fibrosis we used a genetic mouse model expressing a GFP-Cre (GC) fusion protein driven by the FoxD1 promotor (*FoxD1-GC*). In *FoxD1-GC*; *R26R* adult mouse, perivascular interstitial cells can be identified in kidney sections following LacZ staining. As shown in figure 1A and confirming previous studies[1], 10 days after UUO we observed a marked expansion of LacZ positive pericyte-derived myofibroblasts exclusively in the interstitium of the fibrotic kidneys. To allow for cell sorting of kidney cell suspension using FACS sorting of fluorescently labeled pericyte derived cells we subsequently crossed the FoxD1-GC strain with the Z/Red (dsRed) reporter line, which shows a virtually identical expression profile as the FoxD1-GC;R26R strain (Figure 1B). Fibrosis was induced in these FoxD1-GC;Z/Red mice by unilateral ureteric obstruction (UUO) and FoxD1-derivative interstitial cells (dsRed positive) were isolated using FACS sorting from fibrotic kidneys (UUO) vs. contralateral kidneys (CLK). As expected, we observed a marked increase in dsRed positive cells in the kidney after UUO, confirming a marked expansion of in dsRed positive pericyte-derived cells (Figure 1C).

Differential miRNA expression in FoxD1-derivative interstitial cells in fibrosis

To identify miRNAs that are involved in the myofibroblastic response of pericytes in fibrotic kidney disease, we profiled miRNAs from FoxD1-derivative interstitial cells isolated from fibrotic and contralateral control kidneys. This provides a unique miRNA profile of a restricted cell population within an *in vivo* renal injury setting (Figure 1D). As shown in table 1 we found some miRNAs that were previously found to be differentially expressed in fibrosis by profiling miRNAs from whole kidneys, like miR-21[5,14] and miR-214[11]. In addition, we found miR-29 family members to be down regulated, which are known to target collagens[10]. In contrast to previous studies, our approach allowed the identification of miRNAs differentially expressed in pericyte-derive myofibroblasts. Among these, miR-132 stood out as its expression was increased ~21-fold in the myofibroblast compared fractions compared to that of the pericyte control cell suspensions. Also, when validating the upregulation of this miRNA in total kidney (UUO versus CLK; Figure 1E), we observed a 3-4 fold upregulation. To further assess the association of increased miR-132 expression in renal injury we sought to determine if miR-132 would also be differentially regulated in a different renal injury model.

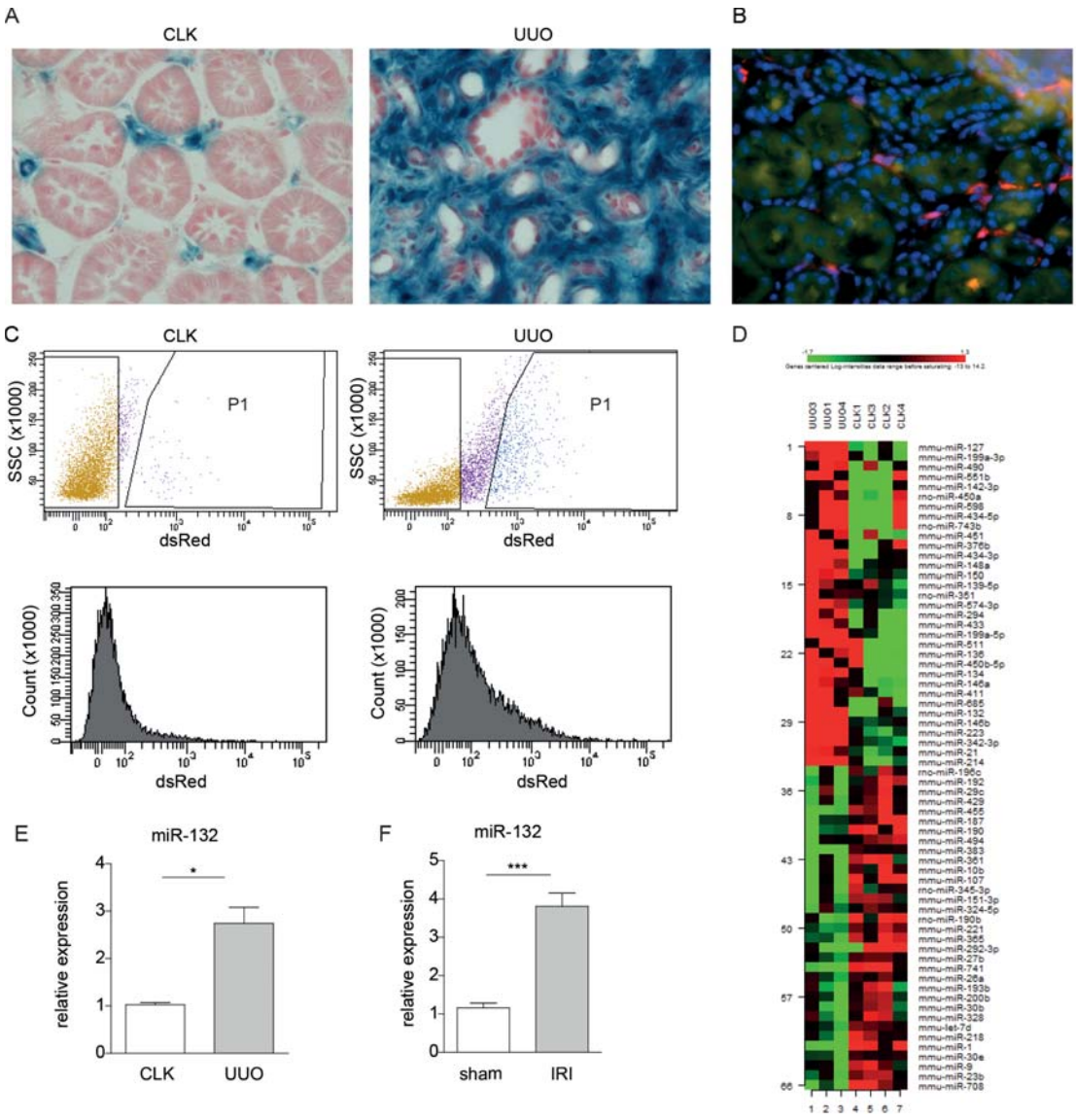

Figure 1. Differential miRNA expression in FoxD1-derivative interstitial cells during fibrosis. A, FoxD1-GC;R26R mice show typical localization of FoxD1 positive cells in mouse kidney visualized by galactosidase expression (LacZ), representing pericytes. UUO induces expansion of FoxD1-derivative myofibroblasts in the interstitium. B, FoxD1-GC;Z/Red mice show similar pericyte specific labeling as compared to FoxD1-GC;R26R mice. C, FACS plots of sorted cells from CLK and UUO kidney. Gated population (P1) represents sorted cell population that are markedly increased after UUO as depicted in the histograms. D, heatmap representing differentially expressed miRNAs with fold change more than 1.3 and p-values lower than 0.17. Red indicates high expression, green low expression. E, qRT-PCR quantification of miR-132 expression in total RNA from UUO kidneys compared to CLK. F, qRT-PCR for miR-132 in total kidney RNA obtained 3 days after renal ischemia reperfusion injury as compared to kidneys from sham operated mice.

Table 1. Differential miRNA expression. Top 20 differentially expressed miRNAs based on p-value. Mean of intensities represents absolute expression level of the miRNA. A positive fold change indicates upregulation in UUO versus healthy kidney. FDR is false detection ratio.

Parametric p-value	FDR	Mean of intensities in CLK	Mean of intensities in UUO	Fold-change	Description
8,80E-06	0,00222	125167,44	1405838,75	11,2	mmu-miR-146b
0,000 5411	0,0668	300290,57	4273538,8	14,3	mmu-miR-223
0,0007948	0,0668	111408,45	658123,93	5,9	mmu-miR-342-3p
0,0036602	0,169	462549,95	3083917,85	6,7	mmu-miR-150
0,0042723	0,169	45198,89	179091	4,0	mmu-miR-574-3p
0,0045003	0,169	382274,52	153939,05	-2,48	mmu-miR-221
0,004864	0,169	81697,22	12130,35	-6,73	mmu-miR-455
0,0054653	0,169	38732,3	828418,64	21,3	mmu-miR-132
0,0060219	0,169	2663,3	244306,59	90,9	mmu-miR-214
0,0078164	0,197	343928,67	176584,64	-1,95	mmu-miR-27b
0,0108911	0,25	166,11	2,42	-68,56	mmu-miR-741
0,0137817	0,274	582439,88	1837951,1	3,1	mmu-miR-21
0,0148108	0,274	1,78	308,9	175,4	mmu-miR-199a -5p
0,0152064	0,274	1099753,64	4653872,5	4,2	mmu-miR-146a
0,019057 5	0,307	37212,5	4528,03	-8,22	mmu-miR-708
0,0202887	0,307	729981,29	177074,88	-4,12	mmu-miR-365
0,0207106	0,307	12843,49	295,09	-43,52	mmu-miR-383
0,0290634	0,398	45829,84	1348570,58	29,4	mmu-miR-685
0,0300052	0,398	5,89	3216,63	555,6	mmu-miR-134
0,0391934	0,443	3,89	338,65	90,9	mmu-miR-294

Therefore, we induced ischemia-reperfusion injury in mice, isolated RNA from the kidneys 3 days after injury and measured miR-132 levels. Indeed, also in this renal injury model we found an over three fold upregulation of miR-132 (Figure 1F).

Silencing miR-132 affects Sirt1, Cox2 and α-SMA expression in vitro

MiR-132 has been described to directly target Sirt1[19] and thereby attenuate renal fibrosis through protection from oxidative injury by increasing Cox2 expression[20]. Therefore we assessed whether miR-132 could also play a role in the differentiation of pericytes towards myofibroblasts in renal fibrosis through targeting Sirt1.

Previously we demonstrated that antagomirs can be used to specifically silence miRNA expression both *in vitro* as well as *in vivo*[21]. Here, we employed an antagomir directed to miR-132 to study the effect of miR-132 in renal fibrosis. First, we investigated the role of miR-132 in regulating Sirt1 and Cox2

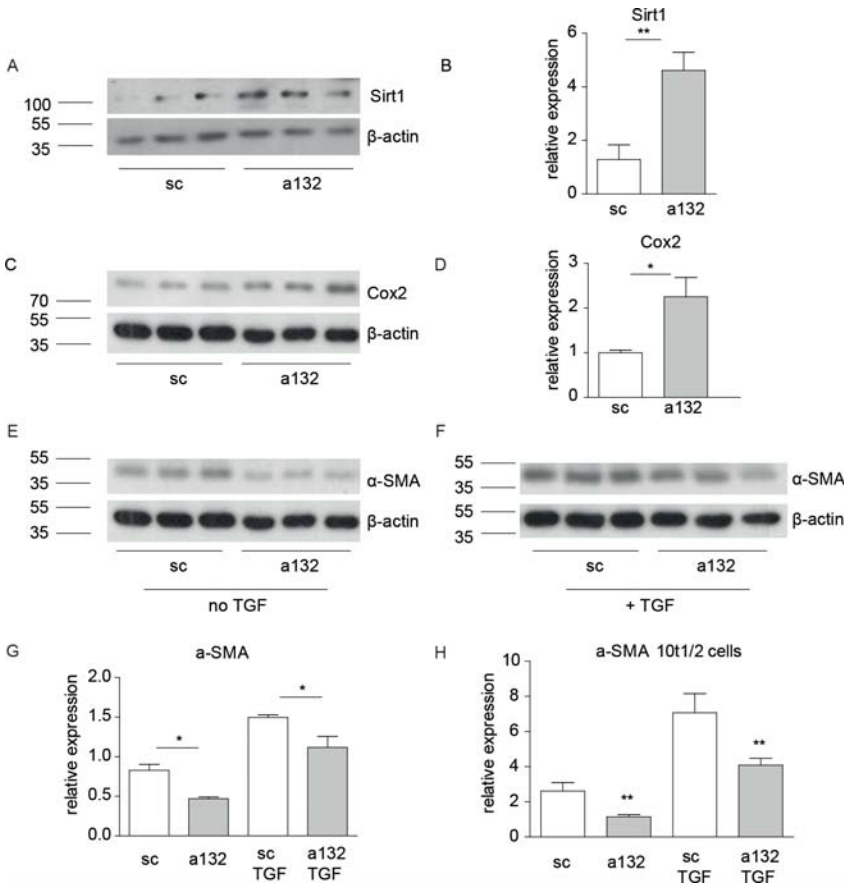

Figure 2. In vitro silencing of miR-132 results in increased Sirt1 and Cox2 expression, while α-SMA is decreased. A, western blot for Sirt1 on NIH3T3 cells treated with antagomir-132 or the scramblemir control. B, Bar graph shows quantification of Sirt1 western blots. C, western blot for Cox on NIH3T3 cells treated with antagomir-132/scramblemir. D, Bar graph shows quantification of Cox2 western blots. All results are normalized on β-actin levels. E and F, western blot for α-SMA of TGF-β stimulated NIH3T3 cells treated with antagomir-132 or the scramblemir control. G, Bar graph shows quantification of α-SMA western blots. Results are normalized on β-actin levels. H, qPCR for α-SMA RNA expression in TGF-β stimulated C3H10T1/3 cells treated with antagomir-132 or the scramblemir control.

expression *in vitro*. When pericyte-like mouse fibroblast cell line (NIH3T3 cells) were cultured in the presence of antagomir-132 for 48 hours both Sirt1 and Cox2 protein expression were increased over two fold as determined by western blot, indicating that antagomir-132 indeed is able to positively affect these proteins (Figure 2A-D).

Cells were then stimulated with TGF-β to induce differentiation towards myofibroblasts. This was evidenced by a change in morphology (elongation; data not shown) and an increase in α-SMA protein expression. The addition of antagomir-132 led to abrogation of this transition as illustrated by a

decrease in morphological alteration (data not shown) and decreased α-SMA protein expression (Figure 2E-G). Note that baseline α-SMA levels are already lowered due to antagomir-132. To confirm this 'anti-fibrotic' effect of antagomir-132, we repeated the experiment on pericyte-like mesenchymal C3H/10T1/2 cells and stimulated them with TGF-β to induce myofibroblast formation. This resulted in increased α-SMA gene expression, which was again decreased when cultured with antagomir-132 (Figure 2H), thereby validating the potential anti-fibrotic role of antagomir-132.

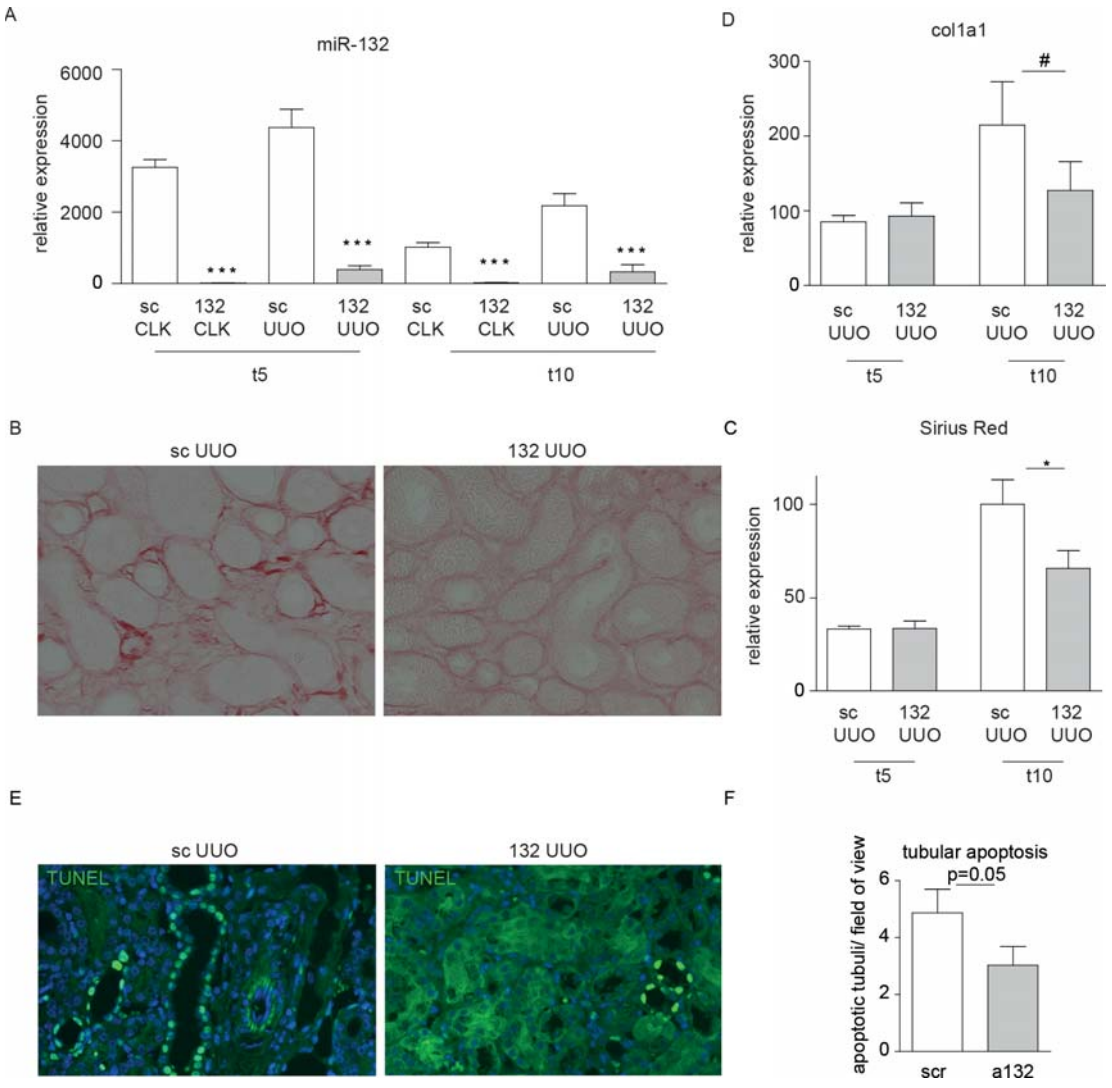

Figure 3. Silencing of miR-132 results in decreased collagen deposition. A, qRT-PCR for miR-132 in total kidney shows silencing of miR-132. B and C, representative microscopic images of Sirius Red staining of UUO kidneys from scramblemir (B) and antagomir-132 (C) treated mice. D, quantification of Sirius Red staining at day 5 and day 10 shows decreased collagen levels at day 10. E, qRT-PCR for collagen1α1. (E and F), representative microscopic images of TUNEL staining (E) and quantification of tubuli containing apoptotic cells (F).

Silencing miR-132 supresses collagen deposition in vivo

Given the antifibrotic effects of miR-132 silencing in vitro, we next investigated the effect of miR-132 silencing in a mouse model of renal fibrosis. Balb/c mice WT mice were administrated with antagomir-132 or scrambled control antagomirs (n=7 per group, 40 mg/kg), exposed to UUO and sacrificed 5 and 10 days after the procedure. Antagomir silencing of miR-132 expression in the treated kidneys was confimed by q-RT-PCR and was found to be almost complete, although in the fibrotic kidneys a low level of expression was retained.

To determine the effect of miR-132 silencing on fibrosis we performed picrosirius red staining to quantify the collagen content in the kidneys. While no difference in kidney collagen content was observed 5 days after UUO, 10 days after UUO we did observe a significant protective effect of miR-132 silencing amounting to a ~25% reduction in collagen deposition (Figure 3A, $p<0.05$). This result was consistent with the reduction of collagen-1α1 gene expression that was not different 5 days after UUO but significantly reduced in the antagomir-132 treated mice 10 days after UUO (Figure 3D, $P= 0.09$). In concordance with the reduced fibrosis, we found a nearly significant reduction in the number of apoptotic tubular epithelial cells, as determined by TUNEL staining, in the antagomir-132 treated cells (Figure 3EF).

Silencing miR-132 reduces the myofibroblast formation 10 days after UUO

To assess the effect of antagomir-132 silencing on UUO induced myofibroblast formation we stained the kidney sections for α-smooth muscle actin (α-SMA). We observed a marked reduction in the number of cells staining positive for α-SMA in kidneys from the mice treated with antagomir-132 as compared to the kidneys of scramblemir-treated mice 10 days after UUO (Figure 4, $p<0.05$). To validate this finding we determined total α-SMA protein expression in these kidneys by western blot. This confirmed the decrease in α-SMA expression in the antagomir-132 treated group at 10 days after surgery (Figure 4CD, $p<0.0005$). Also the α-SMA mRNA levels were consistent with the downregulation of the gene 10 days after UUO (Figure 4E, $p<0.05$). Again no differences in α-SMA expression were observed 5 days after UUO. Since the α-SMA staining directly correlates to the number of FoxD1-derivative interstitial cells[1] we conclude that, following UUO, silencing of miR-132 impacts on the differentiation and/or proliferation of pericytes towards myofibroblasts.

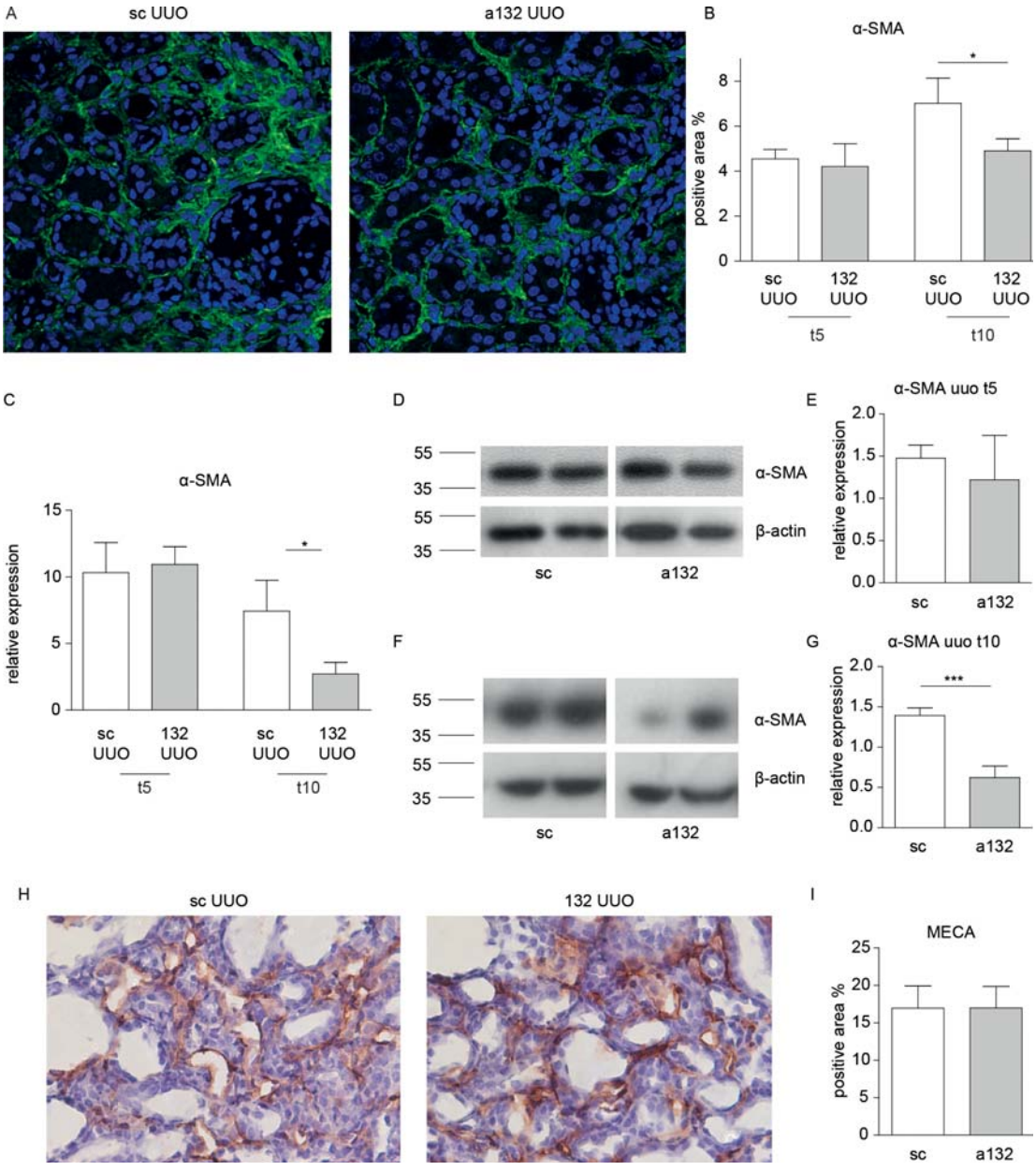

Figure 4. Silencing of miR-132 reduces α-SMA levels 10 days after UUO. A, representative microscopic images of immunofluorescent staining for α-SMA show decreased α-SMA staining in kidneys from mice treated with antagomir-132. B, bar graph shows quantification of α-SMA staining. C, qPCR for α-SMA. D-G, representative duplicate western blots and quantification for α-SMA, normalized by β-actin, in UUO kidneys after 5 days (D and E) and 10 days (F and G). H, no differences in capillary density as illustrated by representative microscopic images of staining for MECA on kidney sections. I, bar graph shows quantification of MECA staining.

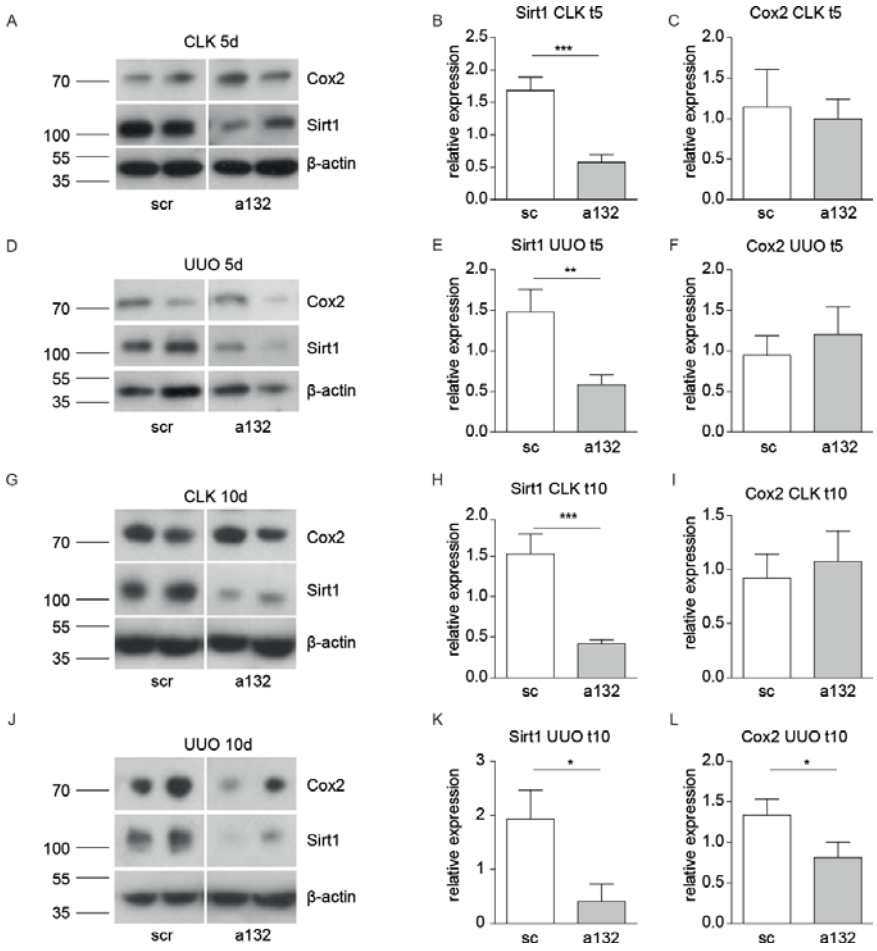

Figure 5. Reduced Sirt1 and Cox2 expression in UUO kidneys of antagomir-132 treated mice. A-L, Western Blot quantification of Sirt1 and Cox2 expression in UUO and control kidneys treated with antagomir-132 or control scramblemir. Bar graphs depict quantified, β-actin normalized Sirt1 and Cox2 expression levels in the treated kidneys.

No difference in capillary density

As the loss of pericytes may be associated with loss of the peritubular capillary network we sought to determine the capillary density in both treatment groups. To that end, we stained whole kidney sections with mouse endothelial cell antigen (MECA). In contrast to our expectation, we did not observe a difference in capillary density between antagomir-132 and scramblemir treated mice 10 days after UUO (Figure 4HI).

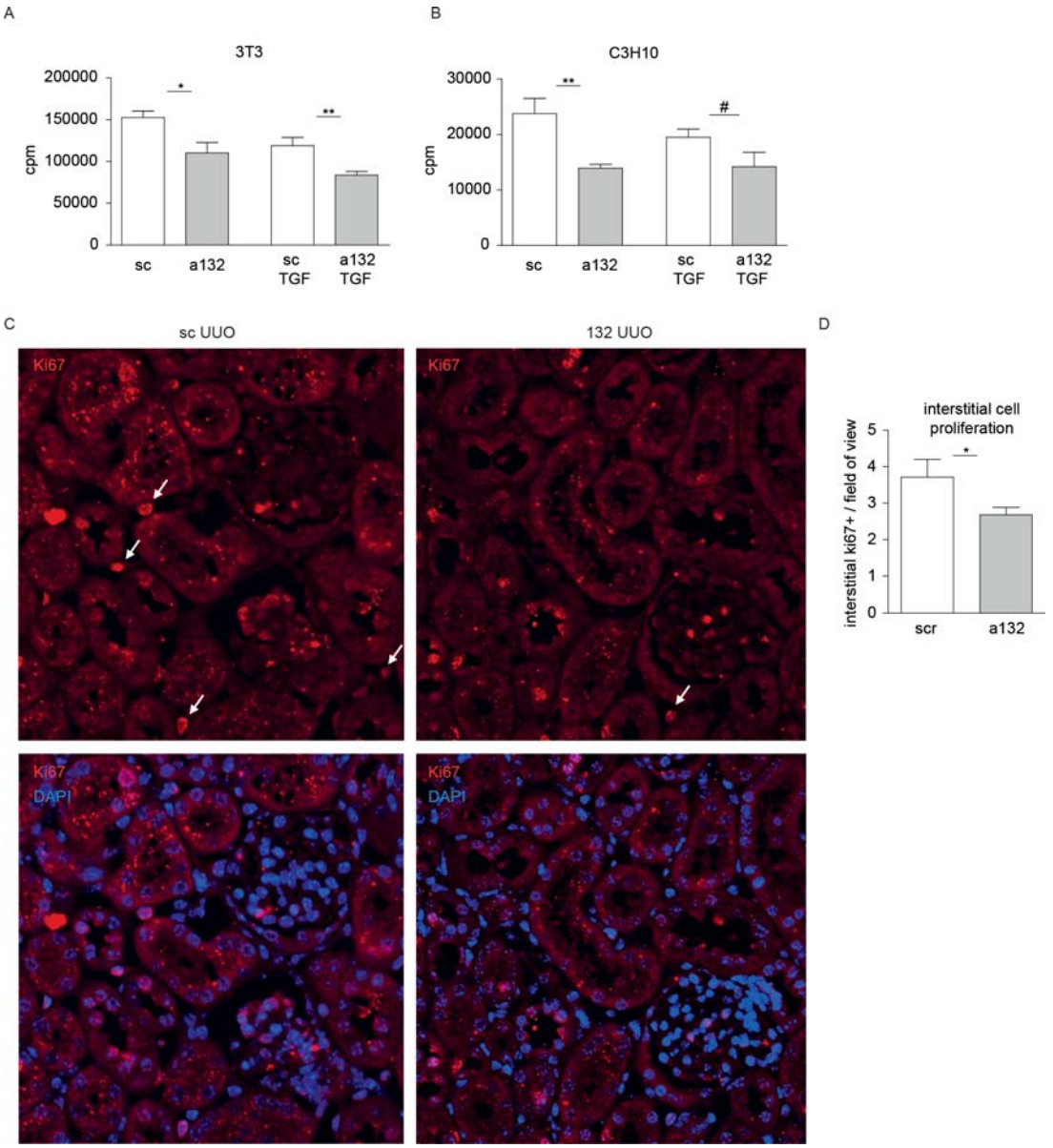

Figure 6. Silencing miR-132 reduces (myo)fibroblast proliferation. Thymidine incorporation proliferations assays demonstrate decreased proliferation of NIH3T3 cells (A) and C3H/10T1/2 cells (B) treated with antagomir-132. Cpm is counts per minute. (C and D), representative microscopic images of Ki67 staining (C) and quantification of Ki67 positive interstitial cells (D) 10 days after UUO in kidneys of mice treated with antagomir-132 or the scramblemir control.

Antagomir-132 decreases levels of Sirt1 and Cox2 in vivo

Following the above, we investigated whether the antifibrotic effects of miR-132 silencing were associated with increased expression of Sirt1 and Cox2. However, in contrast to the effects we observed with myofibroblast formation *in vitro*, miR-132 silencing in UUO kidneys and control kidneys

significantly decreased Sirt1 levels at both timepoints of sacrifice (Figure 5). Cox2 expression was only reduced in the obstructed kidney at day 10 (Figure 5L). This decrease follows the pattern we observed for fibrotic markers that also were decreased only at this time point. Western blot on pooled kidney lysates for each group confirms these findings (Supplementary Figure 1).

Silencing of miR-132 inhibits proliferation of (myo)fibroblasts

As we observed differences in fibrosis only after 10 days, we sought to determine whether miR-132 silencing would affect (myo)fibroblast proliferation. NIH3T3 and C3H/10T1/2 cells were cultured with or without TGF-β and treated with antagomir-132 or scramblemir and proliferation was quantified using the thymidine incorporation assay. Proliferation of both cell lines was significantly reduced when miR-132 was silenced (Figure 6AB). Subsequently we analyzed the number of interstitial proliferating cells in kidney sections from fibrotic kidneys that received either antagomir-132 or scramblemir. Indeed, a decreased number of proliferating cells was observed in the interstitium of antagomir-132 treated kidneys, further supporting a role for miR-132 in (myo)fibroblast proliferation.

Discussion

When mouse kidneys are exposed to UUO, miR-132 expression is strongly increased in the pericyte-derivative myofibroblasts that accumulate during the fibrotic response. As silencing of this microRNA resulted in a decreased fibrotic phenotype of the kidneys 10 days after UUO we conclude that miR-132 plays a rate limiting role in this model of kidney fibrosis. Our data support a facilitary role for miR-132 in the proliferation of myofibroblasts. As myofibroblast are also the mayor contributors to the excessive production of extra cellular matrix proteins, silencing of miR-132 leads to a reduction in the myofibroblastic response as well as to a reduced buildup of collagen-rich scar tissue.

In recent studies aimed at the identification of miRNAs that are involved in the pathogenesis of kidney fibrosis miR-132 was not listed as significantly upregulated in kidneys following UUO, while other common fibrotic miRNAs (mir-21, mir-214, miR-29) were included[14]. We strongly believe this illustrates the value of our approach to use lineage tracing to assess cell type specific miRNA responses that may be masked by the response or influx of numerous other cell types when total kidney RNA preparations are used to identify differentially expressed miRNAs. This is clearly illustrated by the fact that we showed a 21 fold upregulation of miR-132 in the selected FoxD1-derivative cells in obstructed kidneys versus contralateral kidneys while in the RNA preparations from total kidneys miR-132 levels were only 3 fold enriched. Likewise we clearly confirmed suppression of Sirt1 expression by miR-132 *in vitro,* while SIRT1 protein expression in lysates of whole kidneys that were treated with antagomir-132 expression was markedly reduced. Since in this case our measurement involved whole kidney analysis, it is still possible that in the FoxD1-derivatve cells Sirt1 is negatively regulated by miR-132 and the observed decrease is due to the response of other cell types. Although Sirt1 is upregulated in the fibrotic kidney (Supplementary Figure 1), the reduction in SIRT1 expression in the whole kidney extracts is not the result of the reduced fibrotic response in this treatment group as Sirt1 expression is also reduced in the treated contralateral kidneys. Clearly other indirect miR-132 dependent effects may be operational.

The finding that fibrosis is reduced at day 10 only is in concordance with the finding that Cox2 expression is also reduced only in that particular situation. It has been described that Cox2 plays a role in fibroblast differentiation[22], so the lower Cox2 levels might be involved in the reduction of number of

myofibroblasts. It is more likely however that lower Cox2 levels just reflect the decrease in fibrosis as Cox2 is strongly increased during fibrosis (see also Supplementary Figure 1).

It was unexpected that although we observe reduced fibrosis due to miR-132 silencing, this is a 'long-term' effect as after 5 days we did not observe this protective effect. The fact there is no difference in capillary density is also surprising, as peritubular capillary rarefaction is a typical feature of renal fibrosis[23]. In addition, it seems plausible that pericyte to myofibroblast transition could result in detachment of pericytes from the microvascular interface leaving unstable capillaries that would result in rarefaction[2]. These findings suggest an initial phase where pericytes detach from the vessels and transform into myofibroblasts, followed by a proliferation phase of these cells. As we did not observe differences in capillary density, and found the protective effect to take place in a later phase, this suggests miR-132 is not involved in the initial, but in the later proliferating phase. This is supported by the fact that we identified antagomir-132 to be able to suppress proliferation of two different pericyte-like cell lines *in vitro*. In addition, miR-132 silencing has been described to be anti-proliferative in endothelial cells[24] and in saphenous vein-derived pericyte progenitor cells (SVPs)[25]. However, the latter paper also described that SVPs reduce interstitial fibrosis after mycocardial infarction, while this inhibition of fibrosis and reduced cardiac fibroblast proliferation and differentiation into myofibroblasts was abrogated by transfection of SVPs with antimiR-132. These data suggest a dynamic role for miR-132, dependent on source, location and environment.

Taken together, we have demonstrated differential expression of miRNAs in FoxD1-derivative interstitial cells in fibrotic kidneys and show that silencing of miR-132 protects against renal fibrosis. This protection is correlated with a decrease in renal Sirt1 levels and our data suggest an important role for miR-132 in the proliferation of myofibroblasts in renal fibrosis.

Materials and Methods

Cell Culture

The cell lines C3H/10T1/2 and NIH3T3 (mouse fibroblast) were obtained from ATCC (American Type Culture Collection, Manassas, VA). Both cell lines were maintained in Dulbecco's modified Eagle medium (Gibco/Invitrogen, Breda, the Netherlands) supplemented with 10% fetal calf serum (Bio Whittaker/Cambrex, Verviers, Belgium) and 1x L-glutamin (Invitrogen) with a final concentration of 2 mM and were incubated at 37 °C in 5% CO2. Cells were treated with 10 ng/mL TGF-β1 (R&D) for 48 hours unless otherwise indicated. Antagomir-132 or scramblemir was added in a concentration of 5 μg/mL.

Animal experiments

All animal experimental protocols were approved by the animal welfare committee of the veterinary authorities of the Leiden University Medical Center or protocols overseen by Animal Resources and Comparative Medicine at Harvard University.

Bilateral Ischemia Reperfusion Injury of the Kidneys

C57BL/6 WT mice (n=5 per group, age=10 weeks, Charles River, Maastricht, the Netherlands) were used. Before surgery, mice were anesthetized and the core body temperature was maintained at 37 ºC. Via flank incisions the renal artery and vein were identified and bilaterally clamped for 25 minutes using surgical clamps (S&T, Neuhausen, Switzerland). In the sham-group identical surgical procedures were used, except that clips were not applied. After removing the clamps, color change indicating proper reflow was confirmed. After 72 hours the mice were anesthetized and euthanized. Kidneys were removed and RNA was isolated as described elsewhere.

Unilateral Ureteral Obstruction (UUO)

For miRNA profiling of FoxD1-derivative cells, 8 week old FoxD1-GC;Z/Red mice were used. For antagomir studies, 8 week old Balb/c mice WT mice (Jackson Laboratories, Bar Harbor, ME, USA) were used. Unilateral ureteral obstruction (UUO) was performed through a left flank incision under general anesthesia. The ureter was identified and ligated twice at the level of the lower pole of the kidney with two separate silk ties. Antagomir or control scramblemir was administrated i.v. at a dose of 40 mg/kg bodyweight 24 hours before surgery.

Profiling microRNAs by TaqMan® Array MicroRNA Cards

For miRNA cDNA synthesis, total RNA was reverse transcribed using the miRNA reverse transcription kit (Applied Biosystems, Foster City, CA, USA) in combination with the stem-loop Megaplex Human primer pools A V2.1 (Applied Biosystems) according to manufacturer's instructions. For each cDNA sample, 384 microRNAs including 6 controls (RNU44, RNU48, 4*U6), were profiled using TaqMan® Array MicroRNA Human Card A V2.0 (Applied Biosystems) according to manufacturer's instructions. All arrays were run on a 7900HT Fast Real-Time PCR System (Applied Biosystems) and default thermal-cycling conditions. For each array the obtained Ct-values were converted to relative quantities normalized to RNU48.

RNA isolation and qRT-PCR analysis

Total RNA from kidneys was isolated using Trizol reagent (Invitrogen, Breda, The Netherlands). Reverse transcription was performed using a 5 minute 65°C incubation of 250 ng total RNA with dNTPs (Invitrogen) and oligo(dT) (Invitrogen) or using specific Taqman® microRNA probes (miR-132, Applied Biosystems). cDNA was synthesized using a M-MLV First-Strand Synthesis system (Invitrogen). Validation of mRNA levels was carried out using SYBR Green Master Mix (Applied Biosystems). Primer sequences of target genes are as follows: α-SMA (sense) CGTGGCTATTCCTTCGTGAC; α-SMA (antisense): GCGTTCGTAGCTCTTCTCC;Col1α1 (sense): TGACTGGAAGAGCGGAGAGT; Col1α1 (antisense): GTTCGGGCTGATGTACCAGT; GAPDH (sense): ACTCCCACTCTTCCACCTTC; GAPDH (antisense): CACCACCCTGTTGCTGTAG. Levels of expression were determined by normalizing to GAPDH. Validation of miRNA levels was performed using Taqman® miR assays (Applied Biosystems). MiRNA levels were normalized on RNU6B levels obtained from the same RNA. The following primers were used for PCR: U6 (sense) CTCGCTTCGGCAGCACA and U6 (antisense) AACGCTTCACGAATTTGCGT. Results were normalized using Gene Expression Analysis for iCycler IQ® RT-PCR Detection System (Bio-Rad Laboratories, Veenendaal, The Netherlands).

Western Blot

Cells or tissues collected for Western Blot were lysed in RIPA buffer (50mM Tris-HCl pH7.5, 150 mM NaCl, 0.1% SDS, 0.5% sodium deoxycholate, 1mM EDTA, 1% Triton X-100) containing phosphatase and protease inhibitors. Equal amounts of proteins (~20 ug) were prepared in sodium dodecyl sulfate (SDS) sample buffer and boiled for 5 min at 95°C before

loading onto 10% sodium dodecyl sulfate-polyacrylamide (SDS-PAGE) gradient gels, and electrophoresis was carried out under reducing conditions. Proteins were then transferred to nitrocellulose membranes (Amersham, 's Hertogenbosch, the Netherlands) that were blocked overnight with PBS with 0.1% Tween 20 containing 5% nonfat powdered milk and incubated with the primary antibody in this blocking solution for 1 h at room temperature. The blots were subsequently washed in PBS-Tween and then incubated with an appropriate HRP-conjugated secondary antibody in blocking solution. Primary antibodies against the following proteins were used: α-SMA (0.25 ug/mL, R&D, Minneapolis, MN, USA), β-actin (0.1 ug/mL, Abcam, Cambridge, UK), Sirt-1 (1 ug/mL, Abcam) and Cox2 (0.1 ug/mL, Abcam). Horseradish peroxidase conjugated goat-anti-rabbit IgG or goat-anti-mouse IgG (0.05 ug/mL, DakoCytomation, Enschede, The Netherlands) was used as secondary antibody. Bound fragments were detected with chemiluminescent reagents (Supersignal West Dura Extended Duration Substrate; ThermoFisher Scientific, Waltham, MA, USA) and exposed on Hyperfilm ECL (Amersham). Quantitative analysis of the protein bands intensity on Western blot was performed using imageJ software and normalized for β-actin.

Design of Antagomirs

Cholesterol-conjugated RNA analogs, 'antagomirs', (Dharmacon RNA technologies, Lafayette, CO, USA) were synthesized as previously described[26]. For antagomir-132 the following sequence was used: 5'-$c_s g_s$accauggcuguagacug$_s u_s u_s a_s$-Chol-3'. As a control a 'scramblemir' was used, this RNA analog is constructed from a randomized nucleotide sequence which does not bind to any known microRNAs: 5'-$a_s u_s$gacuaucgcuauucgc$_s a_s u_s g_s$-Chol-3'. The lower case letters represent 2'-*O*Me-modified nucleotides; subscript 's' represents phosphorothiate linkage; 'Chol' represents a cholesterol-group linked through a hydroxyprolinol linkage.

Immunohistochemistry

Mice were anesthetized, sacrificed, and immediately perfused via the left ventricle with ice-cold PBS for 2 minutes. Kidneys were sagitally sectioned and half was fixed in 10% neutral buffered formalin at 4°C for 12 hours, processed, embedded in paraffin wax, sectioned, and stained with picrosirius red as follows: the kidney sections were deparaffinized with xylene and then re-hydrated in water through graded ethanol. The slides were then incubated for 5 minutes in 0.2% phosphomolybdic acid (Sigma, St. Louis, MO, USA) to reduce background. The sections were incubated in picrosirius red for three hours followed by a two washes with acidified water. The sections were then

dehydrated and mounted in permount mounting medium (Fisher Scientific, Landsmeer, the Netherlands). Images of complete sections were obtained using a Pannoramic Midi slide scanner (3DHistech, Budapest, Hungary). The area of collagen deposition, stained red by picrosirius red staining, was measured using ImageJ software; whole sections were analyzed. For ki67 staining, after de-paraffinization, sections were subjected to heat-induced antigen retrieval using citrate buffer (10mM, pH 6.0) in a microwave for 20 min. Next, sections were incubated overnight at 4°C with an antibody against Ki67 (Santa Cruz Biotechnology, Santa Cruz, CA, USA) followed by an appropriate secondary antibody labeled with Alexa-488 (Molecular Probes). Apoptotic cells were counted after being identified by the terminal deoxynucleotidyl-transferase-mediated deoxyuridine 5-triphosphate nick end labeling (TUNEL) assay (Roche, Mannheim, Germany).

Other halves of the kidney were fixed in 4% PFA for 1 hour at 4°C, cryopreserved in 20% sucrose, and frozen. 5 μm sections were stained for α-SMA using mouse fluorescein isothiocyanate-conjugated antibody (Sigma). For MECA32, first endogenous peroxidase was blocked with H2O2. Sections were then incubated with a specific antibody against MECA32 (Becton Dickinson, Franklin Lakes, New Jersey, USA), followed by horseradish peroxidase (HRP)-conjugated appropriate secondary antibodies (Jackson Immunoresearch, Westgrove, PA, USA). As a negative control, isotype-matched IgG was used. The staining was visualized using Nova RED (Vector Labs, Peterborough, UK) and counterstained with hematoxylin. Quantification of immunohistochemistry was performed Using image J software, whole sections were analyzed.

FACS sorting

Kidneys were homogenized using a gentleMACS dissociator (Miltenyi Biotec, Bergish Gladbach, Germany) in combination with enzymatic digestion using Liberase (Roche). The obtained cell suspension was sorted using the FACSAria II (BD Biosciences, Franklin lakes, NJ, USA).

Proliferation assay

Proliferation was measured by the addition of ^{3}H-thymidine (0.5 μCi/well; Amersham Biosciences, The Netherlands) 16 hours before cell lysis. The amount of ^{3}H-thymidine incorporation was measured using a liquid scintillation analyzer (Tri-Carb 2900R). Responses are expressed as mean counts per minute of triplicate cultures.

Statistical Analysis

Results are expressed as mean ± standard error of the mean (SEM). Statistical analysis was performed using student's T-test. $P<0.05$ were considered statistically significant.

Supplementary Files

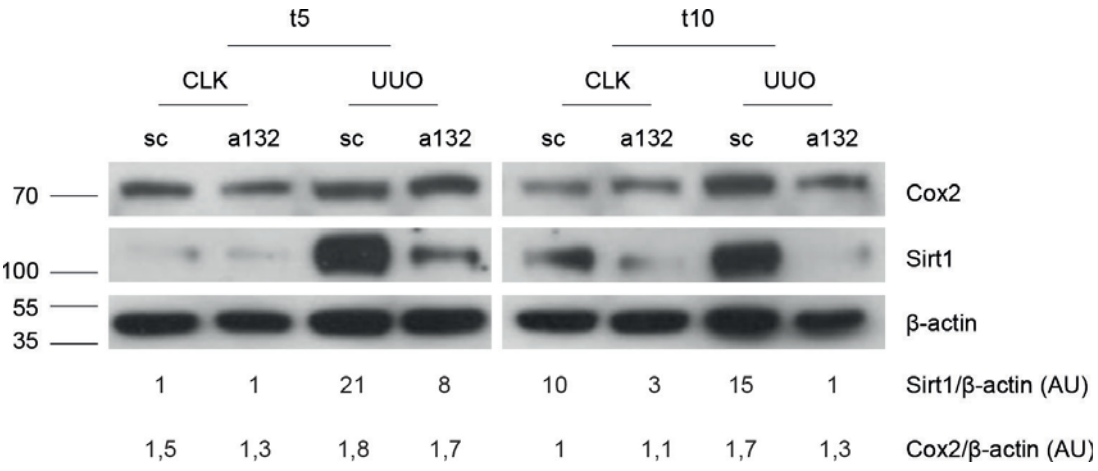

Supplementary Figure 1. Western blot on pooled kidney lysates confirm decrease in Sirt1 due to miR-132 inhibition. Cox2 is only decreased 10 days after UUO. Note that UUO itself results in increased Sirt1 and Cox levels. Below the western blot, Sirt1 or Cox2 over β-actin ratios are indicated.

References

1. Humphreys, B.D., et al. Fate tracing reveals the pericyte and not epithelial origin of myofibroblasts in kidney fibrosis. Am J Pathol 176, 85-97 (2010).
2. Schrimpf, C. & Duffield, J.S. Mechanisms of fibrosis: the role of the pericyte. Curr Opin Nephrol Hypertens 20, 297-305 (2011).
3. Xie, X., et al. Systematic discovery of regulatory motifs in human promoters and 3' UTRs by comparison of several mammals. Nature 434, 338-345 (2005).
4. Kloosterman, W.P. & Plasterk, R.H. The diverse functions of microRNAs in animal development and disease. Dev Cell 11, 441-450 (2006).
5. Thum, T., et al. MicroRNA-21 contributes to myocardial disease by stimulating MAP kinase signalling in fibroblasts. Nature 456, 980-984 (2008).
6. Matkovich, S.J., et al. MicroRNA-133a protects against myocardial fibrosis and modulates electrical repolarization without affecting hypertrophy in pressure-overloaded adult hearts. Circ Res 106, 166-175 (2010).
7. van Rooij, E., et al. Control of stress-dependent cardiac growth and gene expression by a microRNA. Science 316, 575-579 (2007).
8. van Rooij, E., et al. Dysregulation of microRNAs after myocardial infarction reveals a role of miR-29 in cardiac fibrosis. Proc Natl Acad Sci U S A 105, 13027-13032 (2008).
9. Roderburg, C., et al. Micro-RNA profiling reveals a role for miR-29 in human and murine liver fibrosis. Hepatology 53, 209-218 (2011).
10. Liu, Y., et al. Renal medullary microRNAs in Dahl salt-sensitive rats: miR-29b regulates several collagens and related genes. Hypertension 55, 974-982 (2010).
11. Denby, L., et al. miR-21 and miR-214 are consistently modulated during renal injury in rodent models. Am J Pathol 179, 661-672 (2011).
12. Macconi, D., et al. MicroRNA-324-3p promotes renal fibrosis and is a target of ACE inhibition. J Am Soc Nephrol 23, 1496-1505 (2012).
13. Kriegel, A.J., Liu, Y., Cohen, B., Usa, K. & Liang, M. MiR-382 targeting of kallikrein 5 contributes to renal inner medullary interstitial fibrosis. Physiol Genomics 44, 259-267 (2012).
14. Zarjou, A., Yang, S., Abraham, E., Agarwal, A. & Liu, G. Identification of a microRNA signature in renal fibrosis: Role of miR-21. Am J Physiol Renal Physiol (2011).
15. Zhong, X., Chung, A.C., Chen, H.Y., Meng, X.M. & Lan, H.Y. Smad3-mediated upregulation of miR-21 promotes renal fibrosis. J Am Soc Nephrol 22, 1668-1681 (2011).
16. Chung, A.C., Huang, X.R., Meng, X. & Lan, H.Y. miR-192 mediates TGF-beta/Smad3-driven renal fibrosis. J Am Soc Nephrol 21, 1317-1325 (2010).
17. Kato, M., et al. MicroRNA-192 in diabetic kidney glomeruli and its function in TGF-beta-induced collagen expression via inhibition of E-box repressors. Proc Natl Acad Sci U S A 104, 3432-3437 (2007).
18. Krupa, A., et al. Loss of MicroRNA-192 promotes fibrogenesis in diabetic nephropathy. J Am Soc Nephrol 21, 438-447 (2010).
19. Strum, J.C., et al. MicroRNA 132 regulates nutritional stress-induced chemokine production through repression of SirT1. Mol Endocrinol 23, 1876-1884 (2009).
20. He, W., et al. Sirt1 activation protects the mouse renal medulla from oxidative injury. J Clin Invest 120, 1056-1068 (2010).
21. van Solingen, C., et al. Antagomir-mediated silencing of endothelial cell specific microRNA-126 impairs ischemia-induced angiogenesis. J Cell Mol Med 13, 1577-1585 (2009).

22. Frungieri, M.B., Weidinger, S., Meineke, V., Kohn, F.M. & Mayerhofer, A. Proliferative action of mast-cell tryptase is mediated by PAR2, COX2, prostaglandins, and PPARgamma : Possible relevance to human fibrotic disorders. Proc Natl Acad Sci U S A 99, 15072-15077 (2002).
23. Ishii, Y., et al. Injury and progressive loss of peritubular capillaries in the development of chronic allograft nephropathy. Kidney Int 67, 321-332 (2005).
24. Anand, S., et al. MicroRNA-132-mediated loss of p120RasGAP activates the endothelium to facilitate pathological angiogenesis. Nature medicine 16, 909-914 (2010).
25. Katare, R., et al. Transplantation of human pericyte progenitor cells improves the repair of infarcted heart through activation of an angiogenic program involving micro-RNA-132. Circ Res 109, 894-906 (2011).
26. Krutzfeldt, J., et al. Silencing of microRNAs in vivo with 'antagomirs'. Nature 438, 685-689 (2005).